18 September 2025
galgonen@mail.tau.ac.il

FCC-ee Top-up Injection with Multipole Kicker

Gal Gonen[‡†], Sen Yue[†], Yann Dutheil[†]
[‡] Tel Aviv University, Tel Aviv, Israel
[†] CERN, CH-1211 Geneva, Switzerland

Keywords: FCC-ee, multipole kicker injection, particle tracking, Xsuite

Abstract

The FCC-ee (Future Circular e^+e^- Collider) is a proposed next-generation high-luminosity lepton collider designed for precision studies of the Z, W, Higgs, and top quark. To sustain the required luminosity during physics runs, reliable and efficient top-up injection schemes are essential. This study examines the feasibility of Multipole Kicker Injection (MIK) for the FCC-ee lattice, with a particular focus on sextupole- and octupole-based configurations. Particle tracking simulations performed with the Python-based xSuite framework are used to evaluate the impact of kicker strength and Twiss parameter settings on both the injected and circulating beams. The analysis considers injection efficiency, beam survival, and the long-term stability of the stored beam. The results demonstrate that MIK is a promising approach for top-up injection in FCC-ee, while combined multipole kicker schemes may be required to mitigate residual perturbations on the circulating beam.

Contents

1 Introduction

1.1 The FCC-ee and the need for top-up injection

The FCC-ee (Future Circular e^+e^- Collider) is a proposed next-generation high-luminosity lepton collider targeting precision measurements at the Z pole, the W threshold, the Higgs factory mode, and the top-quark threshold. The stored-beam lifetime—limited by processes such as radiative Bhabha scattering and beam–beam interactions—necessitates replenishing the circulating current during physics operation. Defining the instantaneous particle lifetime as

$$\tau_N \equiv -\frac{N}{\dot{N}}, \tag{1}$$

typical values are $\mathcal{O}(10\,\mathrm{h})$ at the LHC but only $\mathcal{O}(1\,\mathrm{h})$ at FCC-ee. To maintain near-constant luminosity under these conditions, the collider must employ *top-up injection*: frequent, minimally perturbative replenishment of the stored beam without interrupting collisions.

1.2 Betatron oscillations, matching, and transverse damping

Transverse motion in a periodic focusing lattice obeys Hill's equation,

$$\frac{d^2x}{ds^2} + K_x(s)\,x = 0, \qquad \frac{d^2y}{ds^2} + K_y(s)\,y = 0, \tag{2}$$

with the standard Twiss-parameter solution

$$x(s) = \sqrt{\beta_x(s)}\,A_x \cos\bigl(\psi_x(s) + \phi_x\bigr), \qquad \psi_x'(s) = \frac{1}{\beta_x(s)}, \tag{3}$$

(and analogously in y). Physically, the particle executes betatron oscillations around the closed orbit with an envelope set by $\beta(s)$. Matching the injected beam's Twiss parameters to the ring optics aligns its phase-space ellipse with the lattice ellipse and reduces capture losses.

Radiation damping reduces oscillation amplitudes turn by turn. Writing the betatron action J (the phase-space area/2π in normalized coordinates), the average decay is

$$J(n) = J(0)\,e^{-nT_0/\tau_{x,y}}, \tag{4}$$

so the rms amplitude decays as $e^{-nT_0/(2\tau_{x,y})}$. Here T_0 is the revolution period and $\tau_{x,y}$ are the transverse damping times. Damping is central to top-up injection: even if the injected beam starts with sizable betatron amplitude, its envelope shrinks toward the closed orbit on the damping timescale.

1.3 Synchrotron radiation essentials

Each turn the beam loses energy U_0 due to synchrotron radiation, and the RF system restores this energy. For the purposes of this study it is sufficient to note the scaling

$$U_0 \propto \frac{E^4}{\rho}, \tag{5}$$

where E is the beam energy and ρ a representative bending radius. Higher energies and tighter bends increase radiation losses and, correspondingly, shorten the characteristic transverse damping times. Throughout this work, transverse betatron amplitudes are treated as damping approximately exponentially with time (or turn number) with ring-specific time constants $\tau_{x,y}$; explicit radiation-integral expressions are not required for the analysis presented here.

1.4 Injection schemes: orbit-bump vs. multipole kicker

Conventional off-axis injection uses a thin septum magnet together with a *local orbit bump* created by fast kickers. The goal is to translate the stored beam closed orbit in the septum region so the injected beam can merge without scraping apertures. A minimal bump can be realized with two thin kickers separated by a betatron phase advance of exactly π, so that the second kicker cancels the net angle outside the bump while producing a parallel translation between the kickers. In practice, four-kicker bumps are often used to relax tolerances and confine the distortion. Any deviation from $\mu = \pi$ (or kicker misbalances) produces residual orbit outside the bump, which can perturb the stored beam and increase backgrounds.

Multipole Kicker Injection (MIK) replaces the conventional dipole kicker with a nonlinear element (e.g., sextupole or octupole) positioned such that the injected bunch, entering with mm-level offset, experiences a strong kick, while the circulating beam near the closed orbit sees a vanishingly small field. This *selectivity* stems from the multipole field scaling, $|B| \propto r^{n-1}$ for order n, so the field and its effective kick go to zero rapidly as $r \to 0$. Thin-lens kicks for sextupole ($S \equiv k_2 L$) and octupole ($O \equiv k_3 L$) illustrate the idea:

$$\text{sextupole:} \quad \Delta x' = -\tfrac{S}{2}(x^2 - y^2), \qquad \Delta y' = S\,xy, \tag{6}$$

$$\text{octupole:} \quad \Delta x' = -\tfrac{O}{6}(x^3 - 3xy^2), \qquad \Delta y' = \tfrac{O}{6}(3x^2 y - y^3). \tag{7}$$

Where for a deflection angle θ and an offset $\tilde{x}$ at the injection point, $k2$, $k3$ are defined:

$$k2 = \frac{2\theta}{\tilde{x}^2}, \quad k3 = \frac{6\theta}{\tilde{x}^3} \tag{8}$$

Near the closed orbit ($x \approx y \approx 0$) these kicks vanish to lowest order, so the stored beam is minimally perturbed; an injected bunch at finite offset samples the nonlinear field and is steered toward the acceptance.

Historical context and adoption Replacing the conventional local-bump scheme with a single pulsed multipole was first explored at the Photon Factory to reduce stored-beam perturbations. The approach matured at BESSY II with the in-vacuum nonlinear kicker (NLK), whose symmetry cancels dipole/quadrupole fields on axis while producing large off-axis kicks for the injected bunch, enabling "transparent" injection. Variants of this MIK/NLK concept have since been deployed or pursued at several light sources (e.g., MAX IV, Sirius, Diamond, SLS-2) and studied for ALS/ALS-U, with design optimizations focused on field shaping, placement, and injected-beam conditions to maximize capture while keeping stored-beam motion minimal [5].

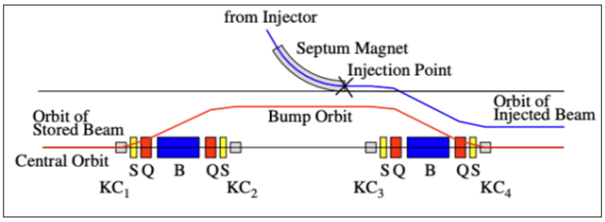

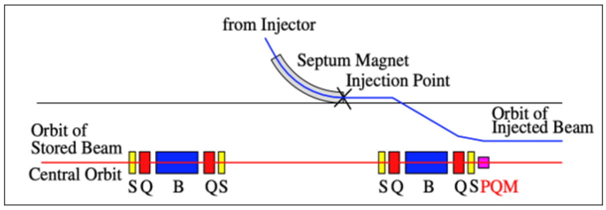

Figure 1: Left: conventional off-axis injection with a local orbit bump (two- or four-kicker scheme, with phase advance $\mu \simeq \pi$ between adjacent kickers). Right: Multipole Kicker Injection (MIK), where a nonlinear element steers the injected bunch while leaving the stored beam nearly unperturbed [7]

1.5 On-axis vs. off-axis injection at FCC-ee

Liouville's theorem (why overlap is nontrivial).

In conservative (Hamiltonian) linear transport the phase-space density is incompressible, so the 4D transverse emittance is preserved and a bright injected beam cannot be "compressed" to overlap the stored beam without either losses or non-Hamiltonian effects. In storage rings, *radiation damping* provides the needed non-Hamiltonian mechanism: the injected beam's betatron action decays exponentially, allowing gradual capture. However, the *instantaneous* transverse acceptance constraints still apply at the injection point, which is why local optics, apertures, and nonlinearities (including MIK) matter.

Definitions (on-momentum vs off-energy).

- **Off-axis (on-momentum) injection:** the injected bunch enters with a controlled transverse offset and/or angle while having $\delta \approx 0$ (same energy as the stored beam). The injected oscillation amplitude then damps toward the closed orbit.
- **On-axis (off-energy) injection:** the injected bunch is placed close to the closed orbit in (x, x', y, y'), reducing initial betatron amplitude. To avoid immediate phase-space overlap, it is commonly injected with a small energy offset $\delta \neq 0$ (separated longitudinally), and, if dispersion is present, a controlled $D_x\delta$ can be used to fine-tune the transverse position. Multipole Kicker Injection (MIK) can assist by steering primarily the incoming bunch while leaving the stored beam nearly unperturbed.

Dynamic Aperture constraint for off axis injection. For off-axis injection to be used, the following condition must be met [6]:

$$5\sigma_{cir} + S + 10\sigma_{inj} < 11\sigma_{cir} \tag{9}$$

However, in FCC-ee, due to the presence of collimators, this requirement is not favored. This constraint motivates on-axis or hybrid injection strategies.

Advantages of on-axis (for FCC-ee). Placing the injected bunch near the closed orbit minimizes initial betatron amplitude, yielding (i) *faster damping* to operational conditions

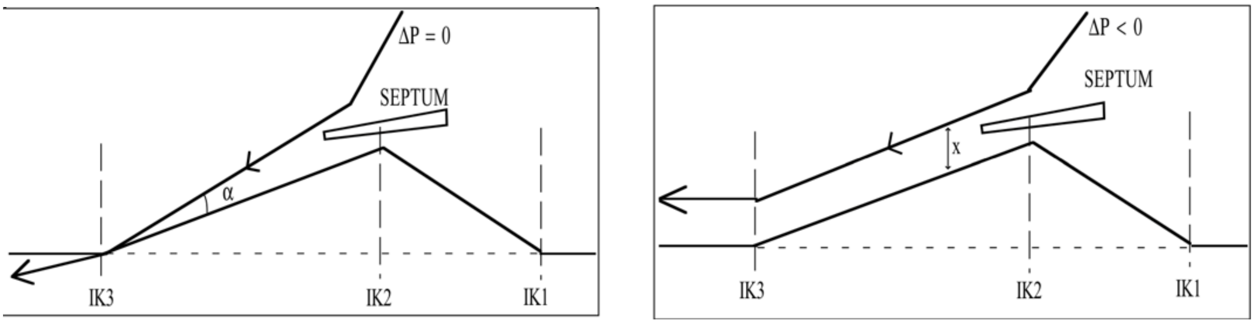

Figure 2: Left: conventional off-axis, on-momentum injection. The Injected beam is injected in an angle α with respect to the circulating beam. Right: On axis (off-momentum) injection scheme, with non-zero dispersion near the septum. Offers faster damping and little radiation damage compared to the off-axis scheme. [2]

and (ii) *lower synchrotron-radiation load* on nearby experiments (reduced large-amplitude oscillations). When combined with MIK, the selectivity of nonlinear kicks further limits perturbations to the circulating beam.

1.6 Key beam-quality concepts

Emittance and beam size. The (geometric) emittance $\varepsilon_{x,y}$ sets the phase-space area of the beam ellipse; with Twiss parameters, the rms size/divergence are

$$\sigma_x = \sqrt{\beta_x \varepsilon_x + (D_x \delta)^2}, \qquad \sigma_{x'} = \sqrt{\gamma_x \varepsilon_x},$$

(and similarly in y), where D_x is dispersion and δ the rms relative momentum spread.

Normalized phase space. We define the Courant–Snyder normalized coordinates. Let

$$X = \frac{x}{\sqrt{\beta_x}}, \qquad P_x = \sqrt{\beta_x}\, x' + \frac{\alpha_x}{\sqrt{\beta_x}} \mathrm{x}, \quad \mathrm{Y}{=}\frac{y}{\sqrt{\beta_y}}, \qquad P_y = \sqrt{\beta_y}\, y' + \frac{\alpha_y}{\sqrt{\beta_y}} y \tag{10}$$

so that linear transport is a rotation and the action $J = \frac{1}{2}(X^2 + P^2)$ is invariant. In this normalized phase space, since the momentum and position values are normally distributed around the values of the reference particle, we expect the beam before MIK to have a circular shape.

Dynamic aperture (DA) and momentum acceptance. The DA is the region of initial transverse phase space that yields stable motion over a specified number of turns; momentum acceptance is the maximal $|\delta|$ sustaining stability (for given amplitudes). Both quantify capture margin and stored-beam robustness in the presence of nonlinearities (including the MIK).

1.7 Aim and scope of this study

This study evaluates sextupole- and octupole-based Multipole Kicker Injection for the FCC-ee lattice using high-statistics tracking. The dependence on integrated multipole strength and on Twiss-parameter configuration at injection is assessed for both injected and circulating beams, with emphasis on injection efficiency, survival, and stored-beam stability (via dynamic-aperture considerations). The results indicate that MIK is a promising approach for FCC-ee top-up injection, while combined multipole kicker configurations may be required to mitigate residual perturbations of the circulating beam.

2 Simulation Setup

2.1 Lattice and optics

All studies were performed on the FCC-ee lattice `GHC_V251`. Unless stated otherwise, optics were computed with the multipole kicker (MIK) turned off and with radiation configured as mean energy loss per turn (no stochastic excitation) in order to obtain a consistent set of Twiss functions for the baseline lattices. All simulations were performed using Xsuite framework [3]. The reference particle was a positron of energy $E_{\mathrm{ref}} = 45.6$ GeV (Z mode). The tune, RF parameters, and relevant magnet settings followed the `GHC_V251` configuration.

2.2 Kicker model and injection geometry

The MIK element was modeled as a *pure* thin multipole, using either a sextupole or an octupole field, without superposed lower-order components. The incoming transfer line was not simulated; instead, at the injection point the incoming bunch was launched with a mean horizontal angle equal to the deflection predicted by the chosen MIK at the tested integrated strength. The MIK was active only on the injection turn (turn 0) and disabled thereafter, so that subsequent motion reflects the ring lattice without further nonlinear kicks from the MIK.

For later reference, the integrated strengths used in the scan are denoted

$$S \equiv k_2 L \quad \text{(sextupole)}, \qquad O \equiv k_3 L \quad \text{(octupole)}, \tag{11}$$

with the corresponding thin-lens kicks given in Eq. 8. $\tilde{x}$ is calculated using the dispersion from the lattice optics at injection point and the energy deviation of the injected beam compared to the circulating beam.

2.3 Source parameters for the injected bunch

The source parameters for both the injected and circulating beams were taken from the booster ring specification and are summarized in Table 1, Table 2. These include the injected geometric emittances ($\varepsilon_{x,\mathrm{inj}}$, $\varepsilon_{y,\mathrm{inj}}$), bunch length $\sigma_{z,\mathrm{inj}}$, and the launch energy offset.

2.4 Radiation and beam–beam models

Tracking was performed with the stochastic quantum radiation model enabled, so that energy loss per turn and photon emission follow the probabilistic treatment provided by the tracking framework. When beam–beam effects were included, a weak–strong bi-Gaussian beam–beam kick was applied at the interaction point together with a beamstrahlung emission model.

2.5 Injected and circulating distributions at the injection point

Unless otherwise noted, the injected bunch was defined to be *achromatic* at the injection point (no transverse dispersion):

$$D_x = D_y = 0, \qquad D'_x = D'_y = 0.$$

Table 1: Injected-beam source parameters from the booster [1]

Quantity	Symbol	Value
Horizontal emittance	$\varepsilon_{x,\mathrm{inj}}$	$1.22 * 10^{-10}$
Vertical emittance	$\varepsilon_{y,\mathrm{inj}}$	10^{-11}
Bunch length (rms)	$\sigma_{z,\mathrm{inj}}$	$2.43 * 10^{-3}$
Energy spread	δ_{inj}	$3.86 * 10^{-4}$

Table 2: Circulating-beam source parameters [4]

Quantity	Symbol	Value
Horizontal emittance	$\varepsilon_{x,\mathrm{cir}}$	$7.1 * 10^{-10}$
Vertical emittance	$\varepsilon_{y,\mathrm{cir}}$	$2.1 * 10^{-12}$
Bunch length (rms)	$\sigma_{z,\mathrm{cir}}$	$1.52 * 10^{-2}$
Energy spread	δ_{cir}	$1.15 * 10^{-3}$

The Twiss parameters (β, α) at the injection point were taken from a 6D Twiss computation of the ring lattice (with radiation in mean mode and MIK off). Let

$$\gamma \equiv \frac{1+\alpha^2}{\beta}.$$

The injected 6D phase-space vector $\mathbf{z} = (x,\, x',\, y,\, y',\, \zeta,\, \delta)^\top$ is sampled from a multivariate normal distribution with mean μ_{inj} and covariance Σ_{inj}:

$$\mathbf{z} \sim \mathcal{N}\big(\mu_{\mathrm{inj}},\, \Sigma_{\mathrm{inj}}\big), \qquad \Sigma_{\mathrm{inj}} = \begin{pmatrix} \varepsilon_{x,\mathrm{inj}}\beta_x & -\varepsilon_{x,\mathrm{inj}}\alpha_x & 0 & 0 & 0 & 0 \\ -\varepsilon_{x,\mathrm{inj}}\alpha_x & \varepsilon_{x,\mathrm{inj}}\gamma_x & 0 & 0 & 0 & 0 \\ 0 & 0 & \varepsilon_{y,\mathrm{inj}}\beta_y & -\varepsilon_{y,\mathrm{inj}}\alpha_y & 0 & 0 \\ 0 & 0 & -\varepsilon_{y,\mathrm{inj}}\alpha_y & \varepsilon_{y,\mathrm{inj}}\gamma_y & 0 & 0 \\ 0 & 0 & 0 & 0 & \sigma_{z,\mathrm{inj}}^2 & 0 \\ 0 & 0 & 0 & 0 & 0 & \sigma_{\delta,\mathrm{inj}}^2 \end{pmatrix}.$$

By "achromatic" we mean that Σ_{inj} contains no x–δ or x'–δ correlations. The mean is placed on the off-momentum closed orbit and includes the MIK kick:

$$\mu_{\mathrm{inj}} = \begin{bmatrix} D_x\,\delta_{\mathrm{inj}} \\ D'_x\,\delta_{\mathrm{inj}} + \theta_{\mathrm{MIK}}(S, O) \\ 0 \\ 0 \\ 0 \\ \delta_{\mathrm{inj}} + \delta_{\mathrm{co}} \end{bmatrix}.$$

In words, we initialize an achromatic beam packet whose centroid coincides with the closed orbit at the injection momentum offset δ_{inj}; the tested MIK kick is then included as an additional mean horizontal angular deflection θ_{MIK}.

Circulating-beam distribution
The circulating beam is matched to the Twiss calculation at the injection point. The emittance is a result of the lattice structure; its specific values (as well as the values for the bunch length and energy spread) are given at Tab.2. Due to energy tapering we get:

$$\langle x \rangle = 0, \quad \langle x' \rangle = 0, \quad \langle y \rangle = \langle y' \rangle = \langle \zeta \rangle = 0, \quad \langle \delta \rangle = 0.$$

2.6 Tracking protocol

At turn 0, the MIK kick was applied and the injected and circulating particles were tracked through the lattice. From turn 1 onward the MIK element was disabled. Each working point and strength configuration was tracked for N_{turn} turns (value specified with the results), recording injection efficiency and survival, emittance evolution, and selected dynamic-aperture . Beam-beam and beamstrahlung effects, when enabled, were applied at the designated interaction point(s).

3 Results

3.1 MIK Influence on the Injected and Circulating Beams

Influence on the injected beam.

Before the MIK, the momentum and position of the injected beam satisfy the following relations:

$$\langle x \rangle \;=\; D_x\,\delta_{\text{inj}}, \qquad \langle x' \rangle \;=\; D'_x\,\delta_{\text{inj}} + \,\theta_{\text{MIK}}(S,O)\;, \qquad \langle y \rangle \;=\; \langle y' \rangle \;=\; \langle \zeta \rangle \;=\; 0 \tag{12}$$

And after it acts on the beam, only the momentum changes:

$$\langle x' \rangle \;=\; D'_x\,\delta_{\text{inj}} \tag{13}$$

However, due to the non-linear nature of the MIK field, the injected beam distribution becomes strongly distorted, as illustrated in figures 3, 4. The distortion is significantly more pronounced in the case of the octupole, as expected, and this effect is also reflected in the subsequent injection efficiency results.

Influence on the stored beam

In an ideal MIK scheme the on-axis field vanishes, so the circulating beam should remain unaffected. In practice, several effects limit this selectivity: (i) the stored beam has finite transverse size and small closed-orbit offsets, so particles sample nonzero multipole fields (sextupole/octupole fields scale with radius and are zero only exactly on axis); and (ii) pulse nonidealities (rise/fall time, leakage, and timing jitter) leave residual fields during the passage of the stored bunch.

Figures 5-6 shows the circulating beam's phase space before and after the MIK. We can clearly see the non linear MIK's influence, parabolic for sextupole and similar to x^3 for octupole.

3.1.1 Emittance Study

The rms emittance is defined:

$$\varepsilon_{x,\text{rms}}^{(5\sigma)} = \sqrt{\langle x^2 \rangle_{5\sigma}\,\langle x'^2 \rangle_{5\sigma} - \langle x x' \rangle_{5\sigma}^2} \tag{14}$$

Here 5σ indicates that we only consider particles whose distance from the point $(\langle x \rangle, \langle x' \rangle)$ is less than 5σ. The evolution of the injected beam emittance as a function of turn, for both the horizontal and vertical phase spaces, is shown in Fig. 7. A sharp increase in the emittance is observed during the first few turns.

A suggested explanation is that the emittance increase results from beam filamentation, i.e., where different regions of the beam oscillate at different frequencies. To examine the beam shape during the first few turns more clearly, we employ normalized phase-space coordinates. The injected beam distribution in normalized phase space is shown in figure 8. As the MIK strength increases, the filamentation becomes more pronounced.

If we continue to use these Twiss parameters (an alternative case with optimized parameters is presented in subsection 3.2.5), it is essential to ensure that the dynamic aperture

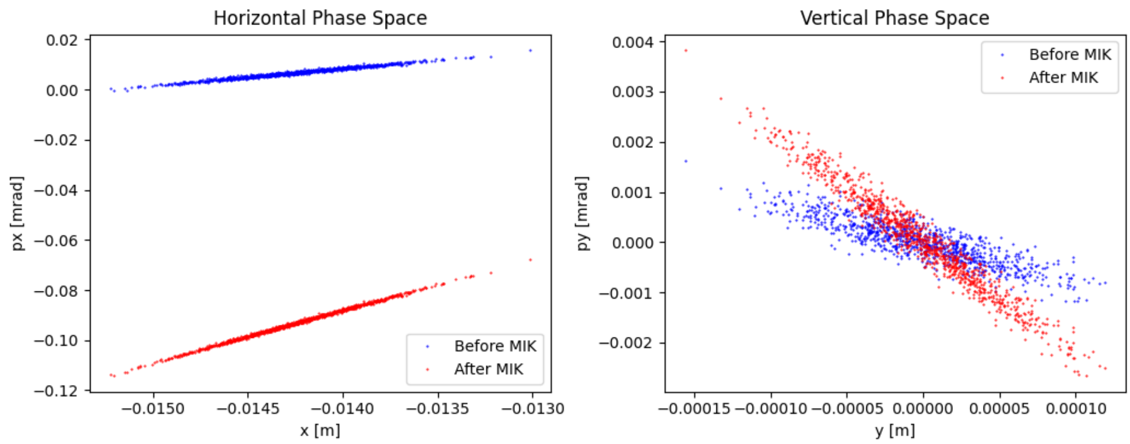

Figure 3: The injected beam phase space before and after the influence of the MIK, $100\mu rad$ Sextupole.

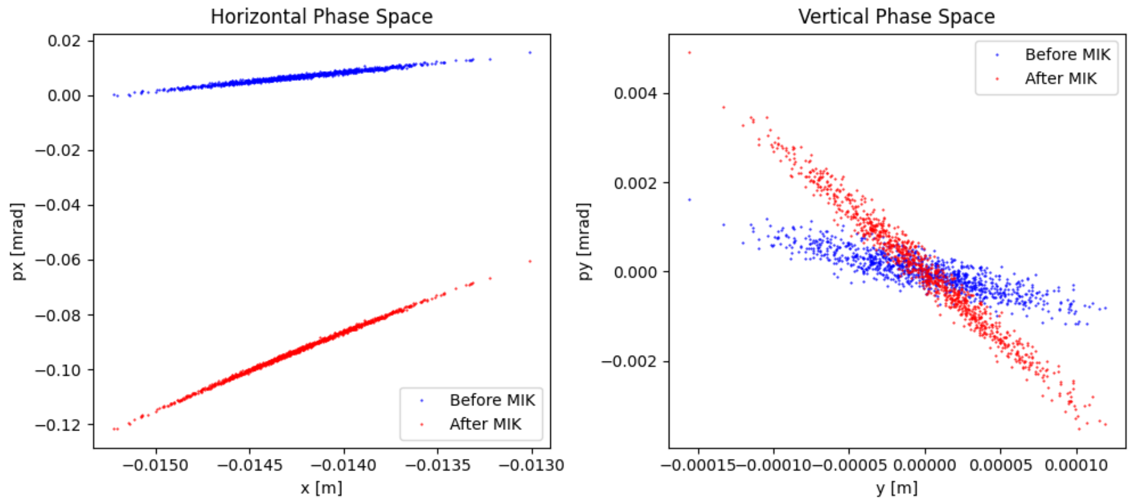

Figure 4: The injected beam's phase space before and after the influence of the MIK, $100\mu rad$ Octupole.

is sufficiently large to contain the filamentation; otherwise, significant beam losses will occur.

As for the circulating beam, its emittance evolution is shown in Fig.9. We can see the increase in the emittance for the first few turns in the horizontal plane, caused by the oscillations and distortions from the MIK influence. These also cause the imperfect survival rate that's discussed in more depth at section 3.3.1.

3.2 Injected Beam Study

3.2.1 Injection efficiency as a function of turn

Injection efficiency is defined on a turn-by-turn basis as the fraction of injected particles that remain within the acceptance. In this study it was evaluated over 100 turns, with 100 circulating particles and 1000 injected particles. An example result is shown in Fig. 10.

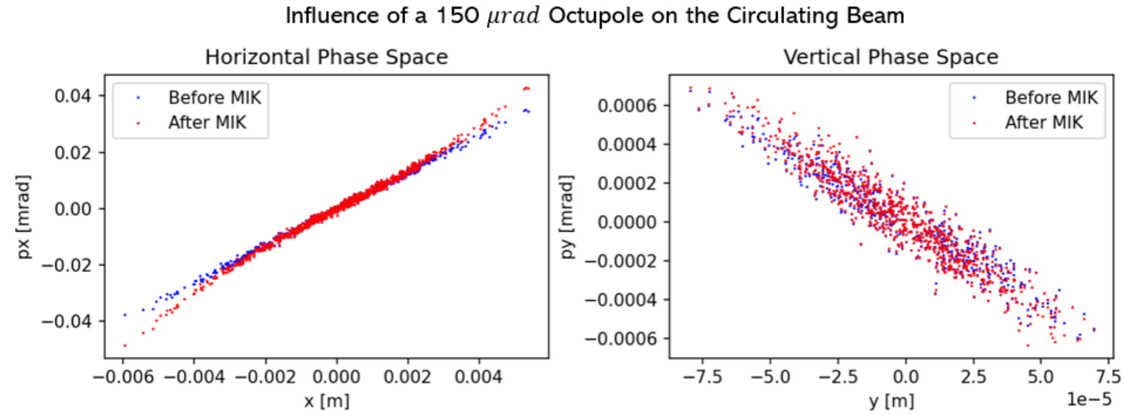

Figure 5: The circulating beam's phase space before and after the influence of the MIK, $150\mu rad$ Octupole.

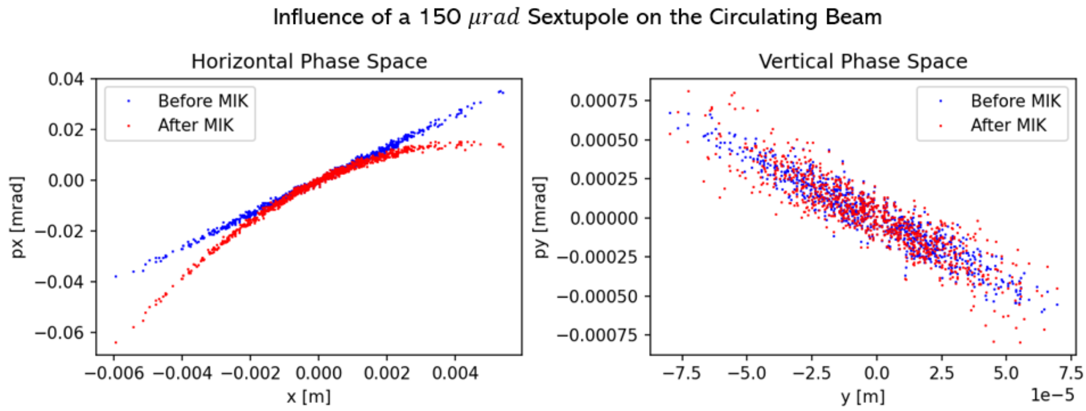

Figure 6: The circulating beam's phase space before and after the influence of the MIK, $150\mu rad$ Sextupole.

3.2.2 Injection efficiency as a function of deflection angle

To investigate the impact of the multipole strength on beam stability, we evaluated the injection efficiency as a function of the deflection angle, as shown in Fig. 11. As expected, the efficiency decreases with increasing multipole strength, with a significantly steeper decline in the octupole case. This behavior arises because stronger multipole kicks introduce larger distortions in the injected beam distribution, leading to a greater fraction of particles exiting the acceptance.

3.2.3 Injection Efficiency as a function of β

We next assess the sensitivity of injection efficiency to the injected beam's Twiss parameters at the injection point. These values are set by the booster–ring matching and can be tuned. In particular, we scanned the horizontal parameters (β_x, α_x), which are expected to have the strongest impact because the MIK kick acts predominantly in x. Unless stated otherwise, the baseline optics at the injection point are $(\beta_x, \alpha_x) = (912, -6.2)$.

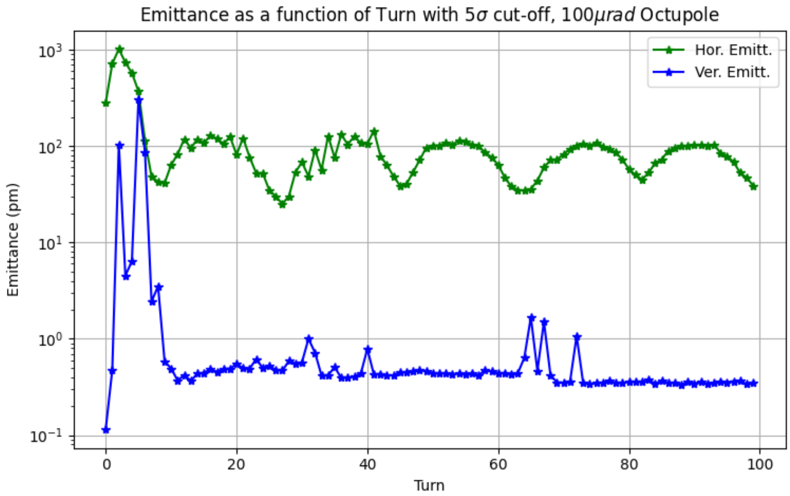

Figure 7: Evolution of the injected beam's horizontal emittance (green) and vertical emittance (blue) by turn.

All scans were performed both *with* and *without* beam–beam effects. When enabled, the beam–beam model consisted of a weak–strong bi-Gaussian beam–beam kick at the injection point together with a beamstrahlung emission model. Inclusion of beam–beam leads to a systematically lower injection efficiency across the scan; however, the difference remains modest, and the location of the optimum is unchanged.

Figure 12 shows the efficiency as a function of β_x for a sextupole kick of 50 μrad, with α_x held at its baseline value -6.2. The efficiency peaks near the optics-matched value from the 6D Twiss at the injection point ($\beta_x = 912\,\text{m}$) and degrades away from it, consistent with mismatch-driven filamentation and larger initial betatron amplitudes. An analogous scan in α_x (Fig. 13), performed with $\beta_x = 912\,\text{m}$, exhibits a different behavior: there the optimal value was nowhere close to the lattice value. Additionally, the efficiency with beam-beam effects wasn't consistently better then without them, although there wasn't a big difference.

3.2.4 Dynamic aperture vs. deflection angle

To determine the conditions for achieving 100% injection efficiency, we evaluated the dynamic aperture (DA) required at the injection point as a function of the MIK deflection angle for both sextupole and octupole configurations. Throughout, DA is reported in units of the injected beam's rms size at the injection point: a value of 5σ corresponds to the radius of the 5σ circle in normalized phase space for the injected beam *before* the MIK acts (see Fig. 14 for the unit convention and visualization).

The resulting DA requirements are shown in Fig. 15 and Fig. 16. As the deflection angle increases, the injection efficiency decreases (see Sec. 3.2.2) and the DA required for 100% capture increases. This trend reflects the stronger phase-space distortion induced by larger MIK kicks, which drive wider early-turn oscillations.

For a given deflection angle, the octupole requires a larger DA than the sextupole, as expected from its stronger nonlinearity and steeper field dependence with radius. Finally, scans performed with and without beam–beam effects show only a modest difference: in-

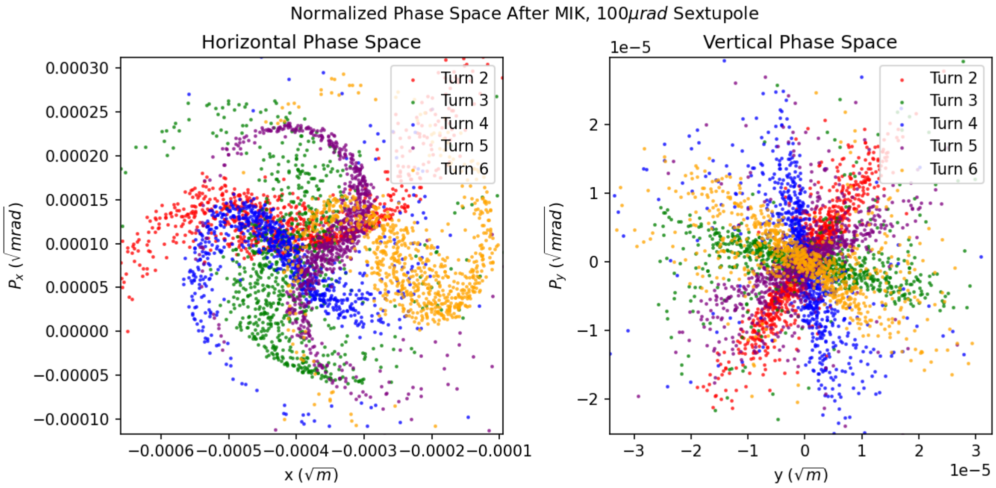

Figure 8: The injected beam's normalized phase space after the MIK influence for the first turns. Left: horizontal phase space, Right: vertical phase space.

Table 3: Baseline versus optimal Twiss parameters for 100 μrad sextupole, no beam-beam effects. The position and momentum dispersions were kept at zero.

Symbol	Baseline Value	Optimal Value
α_x	-6.2	3
α_y	1.7	-0.5
β_x	900.2	820
β_y	206.4	400

cluding beam–beam slightly lowers the efficiency but the qualitative trends and the location of optima are unchanged.

3.2.5 Optimized Twiss parameters for a $100\,\mu$rad sextupole MIK

We investigated whether re-matching the injected beam Twiss parameters at the injection point can improve capture relative to the lattice-derived values. As a test case, we considered a sextupole MIK with a fixed deflection of $100\,\mu$rad, for which the baseline (lattice) Twiss settings yielded an injection efficiency of 75%.

A systematic scan was performed over the four transverse Twiss parameters at the injection point, $(\beta_x, \alpha_x, \beta_y, \alpha_y)$, while keeping the transverse dispersions and their derivatives fixed at zero. The scan objective was to maximize the multi-turn injection efficiency under identical machine and beam conditions (kicker strength, optics, and energy offset).

The optimal settings identified by the scan, together with the corresponding baseline (default) values and the resulting efficiencies, are summarized in Table 3. In the optimum, the injection efficiency increases to 99.8%. Fig. 17 shows the difference in the circulating beam phase space with the different sets of Twiss parameters. Fig. 18 shows the different emittance evolution.

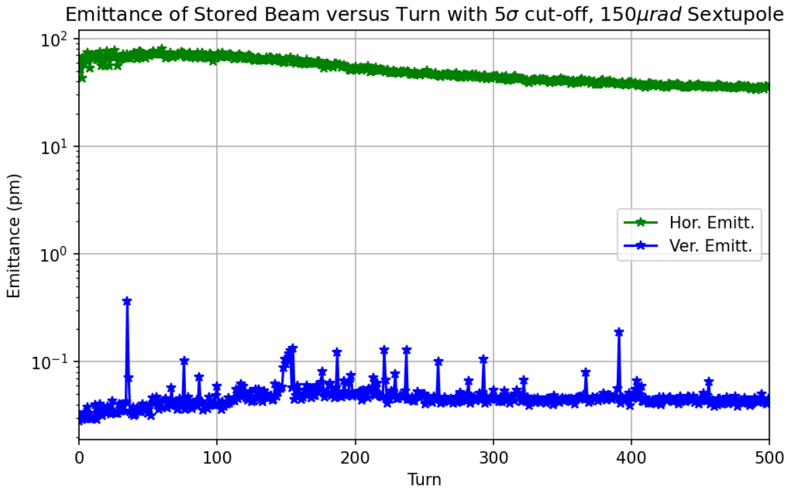

Figure 9: Evolution of the circulating beam's horizontal emittance (green) and vertical emittance (blue) by turn for 150 μrad Sextupole.

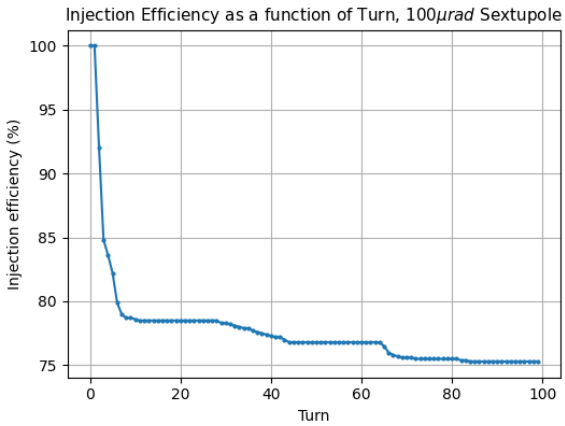

Figure 10: Injection efficiency as a function of turn. The efficiency decreases as particles leave the acceptance region and are lost.

3.3 Circulating Beam Study

3.3.1 Stored-beam survival as a function of MIK deflection angle

Assessing the stored-beam survival as a function of turn is essential, since continuous losses at each injection are unacceptable.

Figure 20 show the survival rate of the circulating beam versus turn for various sextupole and octupole deflection angles, with and without beam–beam effects (weak–strong bi-Gaussian kick with beamstrahlung). Each configuration was tracked with 1000 circulating particles for 2000 turns. As expected the survival rate decreases with increasing deflection angle. However, unlike the case of injection efficiency, for a given angle the sextupole yields lower survival than the octupole. This is consistent with the fact that in this range (of the distance between beams) the octupole field is weaker. Including beam–beam effects produces a modest additional reduction for sextupole but an increased injection efficiency for

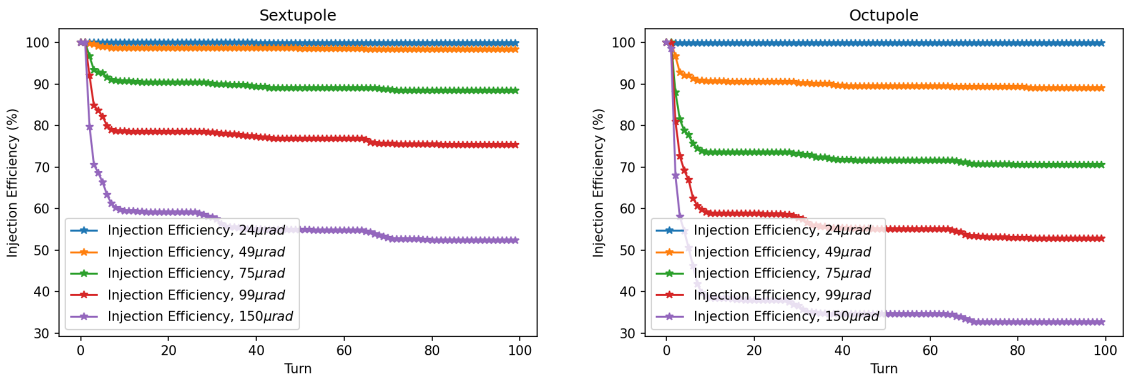

Figure 11: Injection efficiency as a function of deflection angle. Left: sextupole, Right: octupole. The efficiency decreases as particles leave the acceptance region and are lost.

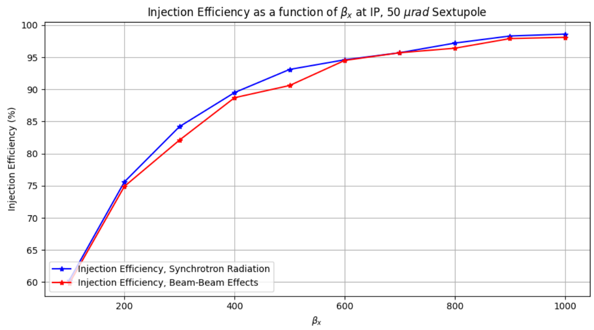

Figure 12: Injection efficiency versus β_x for a sextupole kick of $50\,\mu$rad (with $\alpha_x = -6.2$ fixed). Curves are shown with (red) and without (blue) beam–beam effects; the matched value from the 6D Twiss at the injection point is $\beta_x = 912\,$m.

the octupole; this should be verified, by running the simulation with a larger number of turns.

To better understand the results regarding the beam's survival rate, we looked at the its behavior at the first few turns and its emittance evolution. This behavior is shown in Fig.21. The filamentation in the horizontal plane due to the MIK influence is very pronounced, while in the vertical plane the beam is very stable.

Figure 13: Injection efficiency versus α_x for a sextupole kick of 50 μrad (with $\beta_x = 912$ fixed). Curves are shown with (red) and without (blue) beam–beam effects; the matched value from the 6D Twiss at the injection point is $\alpha_x = -6.2$ m.

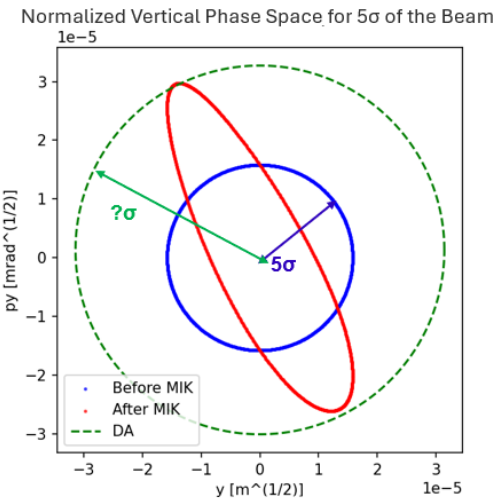

Figure 14: A visualization of the units used to describe the required DA. In blue, 5σ the injected beam in normalized phase space before the MIK. In red, the distorted 5σ line of the beam after the MIK, and in green the required DA after the distortion.

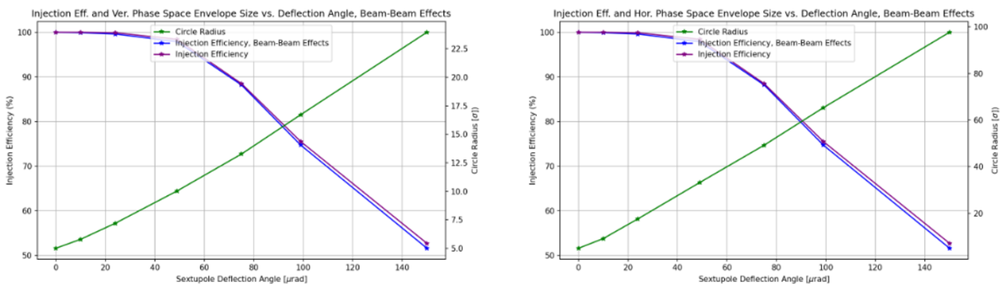

Figure 15: Injection efficiency with (blue) and without (purple) beam-beam effects and the required horizontal and vertical DA at injection point (green) as a function of deflection angle for a sextupole MIK.

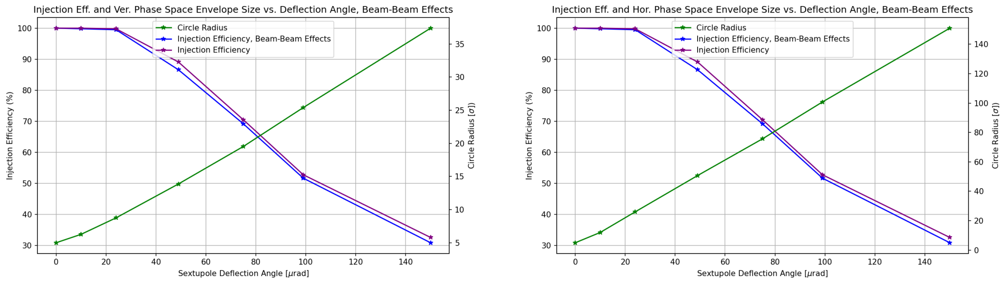

Figure 16: Injection efficiency with (blue) and without (purple) beam-beam effects , the required DA at injection point (green) as a function of deflection angle for an octupole MIK.

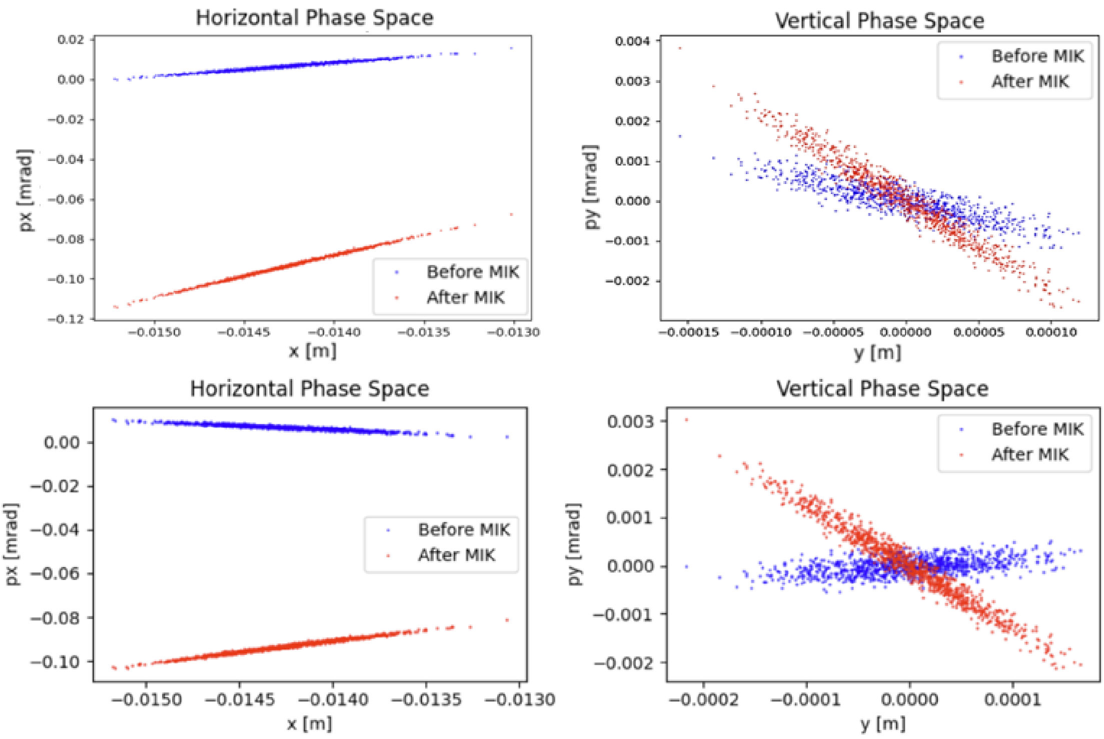

Figure 17: Horizontal and vertical phase space for the circulating beam with baseline versus optimal Twiss parameters

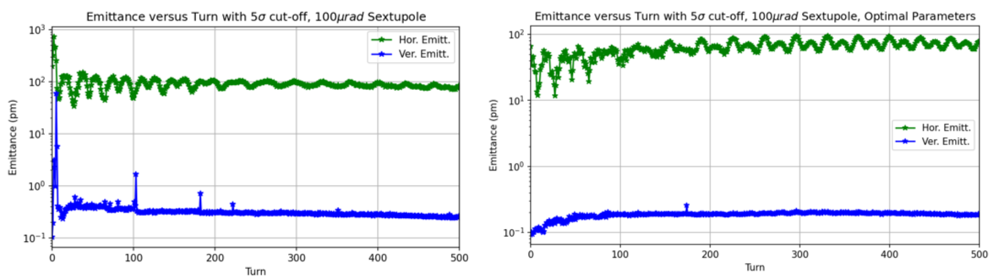

Figure 18: Top: Emittance evolution with baseline parameters, Bottom: Evolution with the optimal parameter set.

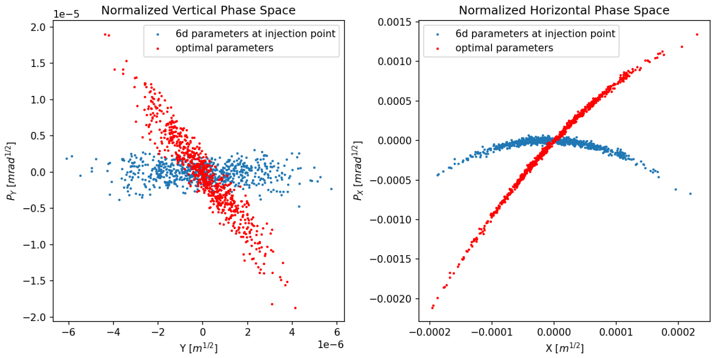

Figure 19: Horizontal and vertical phase space for the injected beam before MIK with baseline vs. optimal twiss parameters

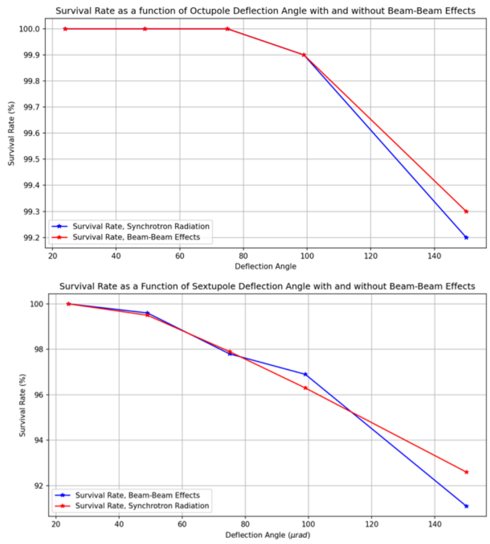

Figure 20: Survival rate of the circulating beam with (blue) and without (red) beam-beam effects as a function of the sextupole (top) and octupole (botton) deflection angle.

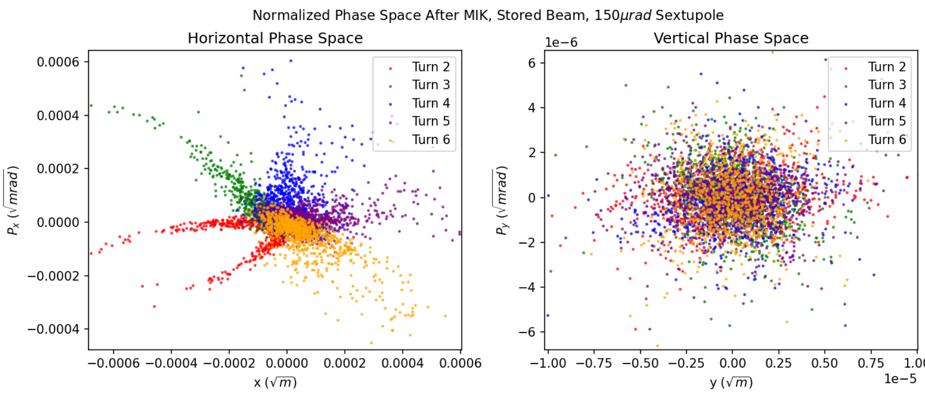

Figure 21: Behavior of the circulating beam in the horizontal and vertical plane for the first few turns. The beam is very stable in the vertical plane while in the horizontal plane we see clear filamentation.

4 Conclusions

Based on the conducted study of injection efficiency, the use of a multipole injection kicker (MIK) appears promising for FCC-ee. The results show, however, that injection efficiency was consistently lower when using the octupole MIK compared to the sextupole configuration. For the test case of a 100 μrad sextupole, the Twiss parameter scan demonstrated that adjusting the injected beam's Twiss parameters in the booster can significantly improve injection efficiency, underlining the importance of upstream beam matching.

The simulations further indicate that beam filamentation, in both the vertical and especially the horizontal plane, increases with MIK strength. This effect must be carefully accounted for when predicting losses: the stronger the MIK, the larger the required dynamic aperture (DA). If the required DA for a given MIK strength exceeds the FCC-ee's available DA, beam losses become unavoidable.

Beam–beam interactions were found to have only a minor impact on injection efficiency, resulting in slightly lower values, which is encouraging for collider operation. By contrast, the circulating-beam study revealed more critical challenges: the nonlinear effects of the MIK appear significant, suggesting that a compensation MIK (CMIK) will be required. The design and testing of such a CMIK should therefore be pursued in future studies.

Finally, the present sextupole and octupole field configurations are unlikely to be optimal. More refined MIK field shapes could be engineered to act more uniformly on the injected beam while minimizing their adverse effects on the circulating beam. Exploring such optimized designs will be an important next step.

References

[1] CERN Accelerator Beam Transfer Group. FCC-ee Booster parameter table. https://gitlab.cern.ch/acc-models/fcc/fcc-ee-heb/-/blob/V24_FODO/Booster_parameter_table.xlsx.

[2] Paul Collier. Synchrotron phase space injection into LEP. *CERN Document Server*, 1996.

[3] Giovanni Iadarola et al. Xsuite: An Integrated Beam Physics Simulation Framework. *JACoW*, HB2023:TUA2I1, 2024.

[4] K. Oide. Optics Oide 250212. https://indico.cern.ch/event/1498712/contributions/6350577/attachments/3012886/5313221/Optics_Oide_250212.pdf. Presented at FCC-ee optics meeting, CERN, 12 Feb 2025.

[5] C. Sun, Ph. Amstutz, T. Hellert, S. C. Leemann, C. Steier, C. Swenson, and M. Venturini. Optimizations of nonlinear kicker injection for synchrotron light sources. *Physical Review Accelerators and Beams*, 23(1):010702, 2020.

[6] Sen Yue. Injection optics for 4ip lattice. Presentation at 175th FCC-ee Optics Design Meeting & 46th FCCIS WP2.2 Meeting, CERN, December 2023. Dec 8, 2023. Slides available via Indico.

[7] Sen Yue. Current status of nonlinear kicker injection. Presentation at "Current status of Nonlinear kicker injection", Indico event (CERN), 2025. Slides available via Indico.